Single-molecule magnet properties of a monometallic dysprosium pentalene complex

Alexander F. R. Kilpatrick,[a] Fu-Sheng Guo,[b] Benjamin M. Day,[b] Akseli Mansikkamäki,*[c] Richard A. Layfield*[a] and F. Geoffrey N. Cloke*[a]

The pentalene-ligated dysprosium complex [(η^8-Pn†)Dy(Cp*)] ($\mathbf{1_{Dy}}$) (Pn† = [1,4-(^{i}Pr$_3$Si)$_2$C$_8$H$_4$]$^{2-}$) and its magnetically dilute analogue are single-molecule magnets, with energy barriers of 188(11) cm^{-1} and 245(28) cm^{-1}, respectively. Whilst the [Cp*]$^-$ ligand in $\mathbf{1_{Dy}}$ provides a strong axial crystal field, the overall axiality of this system is attenuated by the unusual folded structure of the [Pn†]$^{2-}$ ligand.

Single-molecule magnets (SMMs) are coordination compounds that display a magnetic memory effect and an effective energy barrier (U_{eff}) to flipping of their magnetic dipoles.[1] Such materials have, thus far, proven to be of significant fundamental interest, however some SMMs have been incorporated into nanoscale molecular spintronic devices.[2] Ligand design continues to be a key strategy for addressing the properties of SMMs, particularly increasing the temperature at which slow magnetic relaxation can be observed. Synthetic approaches to the design of d- and f-block SMMs are dominated by Werner-type coordination chemistry,[3] however the organometallic approach to SMMs has led to some eye-catching recent examples.[4,5] Within the context of lanthanide SMMs, well-known organometallic ligands such as cyclopentadienide, [Cp]$^-$,[6,7] cyclooctatetraenide, [COT]$^{2-}$,[8] and cycloheptatrienide, [C$_7$H$_7$]$^{3-}$,[9] have been used to influence the properties of dysprosium- and erbium-containing SMMs. In several notable examples, theoretical studies have provided detailed insight into how the properties of these organometallic ligands impact upon the electronic structure of the Ln^{3+} cation, leading to striking increases in the magnetic blocking temperature (T_B) and U_{eff}.

In light of the advances made to date using organometallic chemistry, considerable scope remains for exploring other non-classical ligands in the context of single-molecule magnetism, hence we now turn our attention to the dianion of pentalene, i.e. [C$_8$H$_6$]$^{2-}$ or [Pn]$^{2-}$, an aromatic bicyclic ligand consisting of two fused C$_5$ rings. Pentalene coordination chemistry[10] is considerably underdeveloped relative to that of more established π-organometallic ligands such as cyclopentadienide. However, important developments in the synthesis of pentalene pro-ligands have enabled the study of many pentalene complexes, which, in addition to the fundamental interest in their chemistry, have applications in catalysis and small-molecule activation,[11] and as models for metal-containing polymers.[12] When considered in the context of SMM design, pentalene offers a potential complement to cyclopentadienide and cyclooctatetrenide, the electronic structures of which are regarded as providing axial and equatorial crystal fields, respectively, suitable for slow magnetic relaxation based on dysprosium or erbium, respectively.[6-8] In particular, the formal dianionic charge and the η^8-coordination mode of pentalene, combined with the fold angle between the two fused rings,[10] provide a unique platform on which to construct new magnetic materials. We now describe the SMM properties of [(η^8-Pn†)Dy(Cp*)] ($\mathbf{1_{Dy}}$) (Pn† = [1,4-(^{i}Pr$_3$Si)$_2$C$_8$H$_4$]$^{2-}$) and its magnetically dilute analogue, which were synthesized according to Scheme 1.

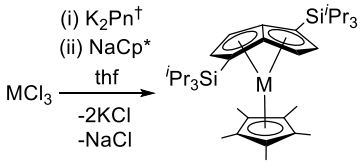

Scheme 1. Synthesis of $\mathbf{1_M}$ with M = Y, Dy.

The addition of one stoichiometric equivalent of K$_2$Pn† to MCl$_3$ (M = Y, Dy) in thf, followed by one equivalent of NaCp*, produced orange solutions from which crystals of $\mathbf{1_{Dy}}$ and $\mathbf{1_Y}$ were isolated in yields of 35% and 30%, respectively. X-ray crystallography confirmed the expected isostructural nature of $\mathbf{1_{Dy}}$ (Fig. 1) and $\mathbf{1_Y}$ (Fig. S4) (Tables S1, S2), with the metal centres being bound to an η^8-Pn† ligand and an η^5-Cp* ligand. The Dy-Pn$_{cent}$ distances of 2.235(3) Å are significantly shorter than the analogous Cp$_{cent}$ distance of 2.344(5) Å ('cent' denotes the centroid of a C$_5$ ring). The Dy–C distances to the

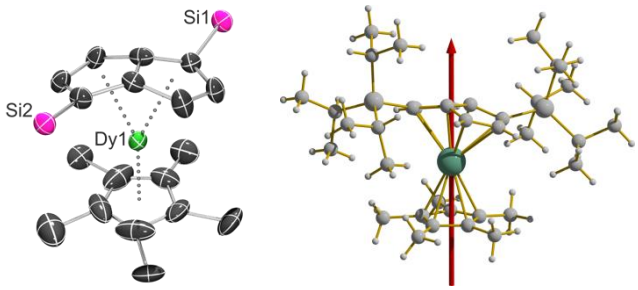

Fig. 1 Left: Thermal ellipsoid representation (50% probability) of the molecular structure of $\mathbf{1_{Dy}}$ (with H-atoms and ^{i}Pr groups omitted for clarity). Right: the principal axis of the **g**-tensor in the ground Kramers doublet of $\mathbf{1_{Dy}}$.

pentalene bridgehead carbon atoms C(4) and C(5) are 2.359(7) Å and 2.371(7) Å, whereas the distances to the wingtip carbons C(2) and C(7) are considerably longer at 2.749(6) Å and 2.731(6) Å, respectively. The Dy–C distances to the carbon atoms in the intermediate positions lie in the range 2.600(6)-2.640(6) Å and the pentalene fold angle is 26.9(4)° (Fig. S5). The range of Dy–C distances to the Cp* ligand is 2.610(9)-2.643(12) Å (average 2.62 Å). The two Pn_{cent}-Dy-Cp_{cent} angles are 152.47(11)° and 153.05(11)°. The dysprosium centre in $\mathbf{1_{Dy}}$ resides 0.200(2) Å above the plane of the three centroids, resulting in a pyramidal coordination environment with approximate C_s symmetry. The shortest intermolecular Dy···Dy distance is 8.8313(8) Å. The solid-state molecular structures of $\mathbf{1_{Dy}}$ and $\mathbf{1_Y}$ are also consistent with the solution-phase structure of diamagnetic $\mathbf{1_Y}$, as confirmed by ^{1}H, ^{13}C and ^{29}Si NMR spectroscopy (Fig. S1-S3).

The magnetic properties of $\mathbf{1_{Dy}}$, which were measured in a static (D.C.) field of 5000 Oe, are typical of a monometallic Dy^{3+} complex with a $^{6}H_{15/2}$ ground term. Thus, the value of $\chi_M T$, where χ_M is the molar magnetic susceptibility, is 13.51 cm^3 K mol^{-1} at 300 K (Fig. S6), which is close to theoretical value of 14.17 cm^3 K mol^{-1}. A gradual decrease in $\chi_M T$ was observed down to about 20 K, at which point a precipitous drop occurred and a value of 7.60 cm^3 K mol^{-1} was reached at 2 K. The overall temperature dependence of the susceptibility is indicative of depopulation of higher-lying crystal field states of Dy^{3+} as the temperature is lowered, followed by the onset of magnetic blocking at very low temperatures. At 1.8 K and 5 K, the magnetization (M) of $\mathbf{1_{Dy}}$ increases rapidly up to fields of about 10 kOe, followed by a more gradual increase at higher fields and reaching values of 5.0 μ_B at 70 kOe (Fig. S6).

The SMM properties of $\mathbf{1_{Dy}}$ were revealed through measurements of the in-phase (χ') and out-of-phase (χ'') A.C. magnetic susceptibility as a function of frequency (ν) (Figs 2 and S7). The $\chi''(\nu)$ plot shows a series of well-defined maxima in the temperature range 2-41 K, with the position of the maxima shifting to higher frequencies as the temperature is raised. Cole-Cole plots of $\chi''(\chi')$ in the same temperature range produced parabola-shaped curves, and fitting of the data with a generalized Debye model yielded α parameters of 0.02-0.22, indicating a narrow distribution of relaxation times. Relaxation times, τ, were extracted from the A.C. susceptibility data and plotted as a function of T^{-1} (Fig. 3), and the data were fitted according to equation 1:

$$\tau^{-1} = \tau_0^{-1} e^{-U_{\text{eff}}/k_B T} + CT^n + \tau_{QTM}^{-1} \qquad (1)$$

In equation 1, τ_0^{-1} and U_{eff} denote the Orbach parameters, C and n denote the Raman parameters, and τ_{QTM}^{-1} is the rate of quantum tunnelling of the magnetization (QTM). The following parameters were extracted for $\mathbf{1_{Dy}}$: U_{eff} = 188(11) cm^{-1}, τ_0 = 2.11 × 10^{-7} s, C = 0.134 s^{-1} K^{-n}, n = 2.74 and τ_{QTM} = 71.07 s. The same analysis on a 5% magnetically dilute sample of $\mathbf{1_{Dy}}$,

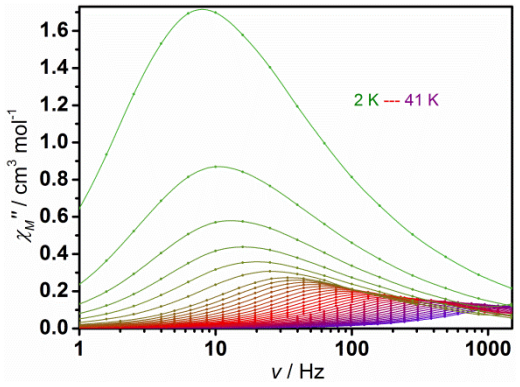

Fig. 2 Frequency dependence of χ'' in zero applied field for $\mathbf{1_{Dy}}$. The solid lines are a guide for the eye.

i.e. $\mathbf{Dy@1_Y}$ produced α parameters of 0-0.39 and U_{eff} = 245(28) cm^{-1}, τ_0 = 4.14 × 10^{-8} s, C = 0.00639 s^{-1} K^{-n}, n = 3.62 and τ_{QTM} = 4.63 s.

Magnetic hysteresis in $\mathbf{1_{Dy}}$ was observed by measuring the field-dependence of the magnetization with a sweep rate of 6.6 Oe s^{-1}. Waist-restricted hysteresis loops were observed up to 2.4 K, although without any coercivity owing to prominent QTM processes. Similar measurements on $\mathbf{Dy@1_Y}$ allowed wider loops with small (e.g. 100 Oe at 1.8 K) coercive fields to be observed up to 3.0 K, which is consistent with the reduced significance of QTM in the diluted sample.

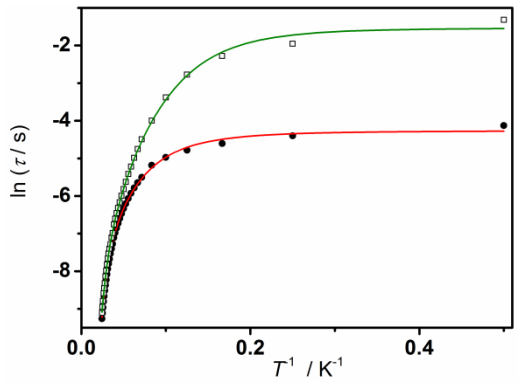

Fig. 3 Temperature dependence of τ for $\mathbf{1_{Dy}}$ (circles) and $\mathbf{Dy@1_Y}$ (squares). Solid red lines represent fits of the data using the parameters stated in the text.

To provide further insight into the magnetic properties, the electronic structure of $\mathbf{1_{Dy}}$ was studied by multi-reference *ab initio* calculations.[13] The coordinates of the heavy atoms were

used in the calculations as determined by X-ray crystallography, and the positions of H atoms were optimized at the DFT level (see ESI for details). The experimental and calculated $\chi_M T(T)$ agree well (Fig. S6), with the calculated $\chi_M T$ value at 300 K being 13.80 $cm^3\ mol^{-1}$ K, compared to the experimental value of 13.51 $cm^3\ mol^{-1}$ K. The deviation is not large (~2%) and most likely results from neglecting electron correlation outside the 4f orbital space in the CASSCF calculations. The most important qualitative feature of the plot, namely, the gradual decrease in $\chi_M T$ upon decreasing the temperature, is correctly produced. The calculated $M(H)$ plots are in very good agreement with experiment (Fig. S6).

The energies of the eight lowest Kramers' doublets within the ground $^6H_{15/2}$ multiplet of **1$_{Dy}$**, along with the principal components of the respective **g**-tensors and the angles between the ground and excited doublets are listed in Table S3. The principal magnetic axis of the ground doublet in **1$_{Dy}$** passes through the centre of the Cp* ligand and the midpoint of the fused pentalene C–C bond (Fig. 1). The ground doublet is almost axial, with a large g_z component and small transverse components, hence the QTM is completely blocked in the ground doublet. The angles between the magnetic axes of the ground doublet and the first three excited doublets are small, and then quickly become perpendicular in the higher doublets. The first excited doublet lies at 197 cm^{-1}, which is quite close to the experimentally observed barrier height of 188 cm^{-1} in **1$_{Dy}$**. In the first excited state, the transverse components of the **g** tensor are still small, but not vanishingly so, and the QTM process is not completely blocked. Based on the experimental evidence, the QTM in this doublet is significant enough such that thermally activated QTM via the first excited doublet is the dominant relaxation mechanism.

The splitting of the $^6H_{15/2}$ multiplets in **1** was studied further by calculating the *ab initio* crystal field (CF) parameters,[14] which are listed in Table S4. The decomposition of the SO-RASSI wave-functions of the sixteen lowest states (eight lowest doublets) into squared projections onto $|JM_J\rangle$ states (where J = 15/2) is given in Table S5. The states in the lowest doublet have large squared projections (0.925) on the M_J = ±15/2 states, as is usual for Dy^{3+} SMMs.[6,7] The M_J states become increasingly mixed as one moves to higher doublets. The first excited doublet has a squared projection of 0.888 on the M_J = ±13/2 state and therefore still approximates to the M_J = ±13/2 states. In higher doublets the correspondence of the SO-RASSI states with a single given M_J state is lost.

The mechanisms for the relaxation of magnetization in **1$_{Dy}$** was studied by constructing the qualitative relaxation barrier using a previously proposed method.[15] Plotting the energies of the lowest states against their respective magnetic moments, with the states being connected by their transition magnetic moment matrix elements, provides the relaxation route corresponding to a pathway traced by the largest matrix elements. The resulting plot (Fig. 4) retains its "barrier-like" structure up to the sixth doublet. Based on the calculations, the most probable relaxation route in **1$_{Dy}$** is an Orbach mechanism via the third excited Kramers doublet at 498 cm^{-1}. However, the experimental data for **1$_{Dy}$** show that the relaxation takes place via the first excited doublet. The QTM in this doublet is weak (roughly an order of magnitude stronger than in the ground doublet), but strong enough to overcome the Orbach route. In addition, the increase in the barrier of approximately 60 cm^{-1} upon dilution implies that Orbach-type relaxation is not the only mechanism, and hence that a Raman process should also contribute.

The anisotropy barriers and hysteresis properties determined for **1$_{Dy}$** and **Dy@1$_Y$** are reminiscent of those found in the series of dysprosium metallocene SMMs reported by some of us,[6,7a] which have very similar Dy–C(Cp) distances to **1$_{Dy}$**. Since Cp ligands in axial positions are known to promote SMM properties in complexes of Dy^{3+}, the bridgehead pentalene carbon atoms, which occupy axial positions and are much closer to the metal centre, should also enhance the magnetic axiality. However, it is noticeable that the other Dy–C(Pn) distances – and the positions of the carbon atoms with respect to the metal centre – are similar to those found in dysprosium complexes of the $[COT]^{2-}$ ligand. Since $[COT]^{2-}$ is thought to diminish the magnetic axiality of the prolate Dy^{3+} ion in, e.g., $[Dy(COT)_2]^-$,[8] we can propose that the non-bridgehead pentalene carbons in **1$_{Dy}$** provide a non-negligible equatorial field and therefore produce an effect similar, yet stronger, to that of COT. Furthermore, the Pn_{cent}-Dy-Cp_{cent} in **1$_{Dy}$** angles are 152.47(11)° and 153.05(11)°, hence they are very similar to the Cp-Dy-Cp angle of 152.845(2)° in $[(Cp^{ttt})_2Dy]^+$, an SMM with a barrier of 1277 cm^{-1} and a T_B of 60 K.[7a] Since the properties of $[(Cp^{ttt})_2Dy]^+$ arise from the exceptional axiality of the ligand environment, the two opposing C_5 rings in the pentalene ligand of **1$_{Dy}$** effectively compete with each other in a way that diminishes the axiality. Hence, **1$_{Dy}$** is an SMM but with a modest barrier and waist-restricted hysteresis. The large, non-axial B_2^2 parameter (Table S4) also explains the significant mixing of the higher-lying Kramers doublets. The principal reason for the magnetic axiality in **1$_{Dy}$** is therefore the relatively large negative axial crystal field parameter B_2^0, whereas the other important axial parameters B_4^0 and B_6^0 are smaller.

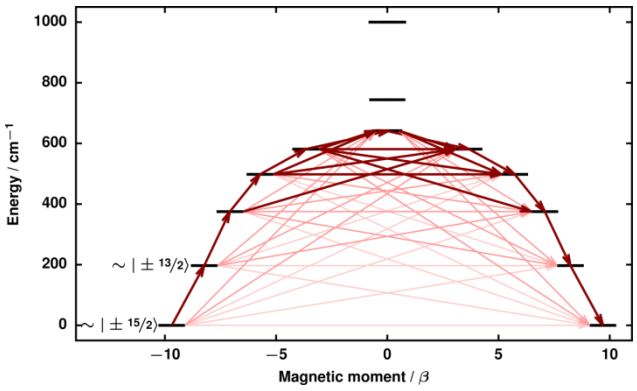

Fig. 4 Calculated magnetic relaxation barrier for **1$_{Dy}$**. Darker arrows indicate the largest matrix elements, indicating the most probable relaxation route.

In summary, the magnetic properties of the first pentalene-ligated SMM have been described. Large anisotropy barriers

were determined for $\mathbf{1_{Dy}}$ and its magnetically dilute analogue, the origins of which were assigned to the strong axial field provided by the $[Cp^*]^-$ ligand and the bridgehead carbon atoms of the $[Pn^\dagger]^{2-}$ ligand. The dominant relaxation process in $\mathbf{1_{Dy}}$ is thermally activated process via the second Kramers doublet. The appreciable equatorial field provided by the non-bridgehead carbon atoms attenuates the U_{eff} value and results in magnetic hysteresis occurring without coercivity. In terms of magneto-structural correlations, the folded nature of the pentalene ligand provides a unique coordination chemistry strategy for addressing the electronic structure of Ln^{3+} cations, and our on-going research will apply this in the design of magnetic, spintronic and optical materials.

The authors thank the European Research Council (AdG grant 247390, CoG grant 646740), the EPSRC (EP/M023885/1, EP/M022064/1), the Academy of Finland (projects 282499, 289172), Prof H. M. Tuononen (University of Jyväskylä) for providing computational resources, and Dr T. Pugh, Prof. R. N. Nair and Dr A. Achari (Manchester) for assistance with magnetic susceptibility measurements.

Conflicts of interest

There are no conflicts to declare.

Notes and references

1 (a) S. K. Gupta and R. Murugavel, *Chem. Commun*., 2018, **54**, 3685. (b) J. Lu, M. Guo and J. Tang, *Chem. Asian J*., 2017, **12**, 2772. (c) J. M. Frost, K. L. M. Harriman and M. Murugesu, *Chem. Sci*., 2016, **7**, 2470. (d) J.-L. Liu, Y.-C. Chen and M.-L. Tong, *Chem. Soc. Rev*., 2018, **7**, 2431.

2 S. Lumetti, A. Candini, C. Godfrin, F. Balestro, W. Wernsdorfer, S. Klyatskaya, M. Ruben and M. Affonte, *Dalton Trans*., 2016, **45**, 16570.

3 (a) C. Papatriantafyllopoulou, E. E. Moushi, G. Christou and A. J. Tasiopoulos, *Chem. Soc. Rev*., 2016, **45**, 1597. (b) D. N. Woodruff, R. E. P. Winpenny and R. A. Layfield, *Chem. Rev*. 2013, **113**, 5110. (c) Y.-C. Chen, J.-L. Liu, L. Ungur, J. Liu, Q.-W. Li, L.-F. Wang, Z.-P. Ni, L. F. Chibotaru, X.-M. Chen and M.-L. Tong, *J. Am. Chem. Soc.,* 2016, **138**, 2829. (d) S. K. Gupta, T. Rajeshkumar, G. Rajaraman and R. Murugavel, *Chem. Sci*., 2016, **7**, 5181. (e) T. Morita, M. Damjanovic, K. Katoh, Y. Kitagawa, N. Yasuda, Y. Lan, W. Wernsdorfer, B. K. Breedlove, M. Enders and M. Yamashita, *J. Am. Chem. Soc*., 2018, **140**, 2995.

4 R. A. Layfield, *Organometallic*s 2014, **33**, 1084.

5 (a) Y. Meng, Z. Mo, B. Wang, Y. Zhang, L. Deng and S. Gao, *Chem. Sci*., 2015, **6**, 7156. (b) T. P. Latendresse, N. S. Bhuvanesh, M. Nippe, *J. Am. Chem. Soc*., 2017, **139**, 14877.

6 (a) R. A. Layfield, J. J. W. McDouall, S. A. Sulway, D. Collison, F. Tuna and R. E. P. Winpenny, *Chem. Eur. J*., 2010, **16**, 4442. (b) T. Pugh, N. F. Chilton and R. A. Layfield, *Angew. Chem. Int. Ed*. 2016, **55**, 11082. (c) T. Pugh, F. Tuna, L. Ungur, D. Collison, E. J. L. McInnes, L. F. Chibotaru and R. A. Layfield, *Nat. Commun*. 2015, **6**, 7492. (d) T. Pugh, V. Vieru, L. F. Chibotaru and R. A. Layfield, *Chem. Sci*., 2016, **7**, 2128. (e) T. Pugh, N. F. Chilton and R. A. Layfield, *Chem. Sci*., 2017, **8**, 2073. (f) F.-S. Guo and R. A. Layfield, *Chem. Commun*., 2017, **53**, 3130. (g) R. Grindell, B. M. Day, F.-S. Guo, T. Pugh and R. A. Layfield, *Chem. Commun*., 2017, **53**, 9990.

7 (a) F.-S. Guo, B. M. Day, Y.-C. Chen, M.-L. Tong, A. Mansikkamäki and R. A. Layfield, *Angew. Chem. Int. Ed*., 2017, **56**, 11445. (b) S. Demir, M. I. Gonzalez, L. E. Darago, W. J. Evans and J. R. Long, *Nat. Commun*., 2017, 8, 2144. (c) S. Jiang, B. Wang, H. Sun, Z. Wang and S. Gao, *J. Am. Chem. Soc.*, 2011, **133**, 4730 (d) Y.-S. Meng, Y.-Q. Zhang, Z.-M. Wang, B.-W. Wang and S. Gao, *Chem. Eur. J*., 2016, **22**, 12724 (e) C. A. P. Goodwin, F. Ortu, D. Reta, N. F. Chilton and D. P. Mills, *Nature,* 2017, **548**, 439. (f) C. P. Burns, B. O. Wilkins, C. M. Dickie, T. P. Latendresse, L. Vernier, K. R. Vignesh, N. S. Bhuvanesh and M. Nippe, *Chem. Commun*., **2017**, *53*, 8419.

8 (a) L. Ungur, J. J. Le Roy, I. Korobkov and M. Murugesu, *Angew. Chem. Int. Ed*., 2014, **53**, 4413. (b) J. J. Le Roy, L. Ungur, I. Korobkov, L. F. Chibotaru and M. Murugesu, *J. Am. Chem. Soc*., 2014, **136**, 8003. (c) J. J. Le Roy, M. Jeletic, S. I. Gorelsky, I. Korobkov, L. Ungur, L. F. Chibotaru and M. Murugesu, *J. Am. Chem. Soc*., 2013, **135**, 3502. (d) K. R. Meihaus and J. R. Long, *J. Am. Chem. Soc*., 2013, **135**, 17952.

9 K. L. M. Harriman, J. J. Le Roy, L. Ungur, R. Holmberg, I. Korobkov and M. Murugesu, *Chem. Sci*., 2017, **8**, 231.

10 F. G. N. Cloke, J. C. Green, A. F. R. Kilpatrick and D. O'Hare, *Coord. Chem. Rev*., 2017, **344**, 238.

11 (a) F. G. N. Cloke and P. B. Hitchcock, *J. Am. Chem. Soc*., 2002, **124**, 9352. (b) A. E. Ashley, A. R. Cowley and D. O'Hare, *Eur. J. Org. Chem.*, 2007, 2239. (b) F. M. Chadwick and D. O'Hare, *Organometallics*, 2014, **133**, 3768.

12 (a) A. F. R. Kilpatrick and F. G. N. Cloke, *Dalton Trans*., 2017, **46**, 5587. (b) G. Balazs, F. G. N. Cloke, J. C. Green, R. M. Harker, A. Harrison, P. B. Hitchcock, C. N. Jardine and R. Walton, *Organometallics*, 2007, **26**, 3111.

13 F. Aquilante, J. Autschbach, R. K. Carlson, L. F. Chibotaru, M. G. Delcey, L. De Vico, I. Fdez. Galván, N. Ferré, L. M. Frutos, L. Gagliardi, M. Garavelli, A. Giussani, C. E. Hoyer, G. Li Manni, H. Lischka, D. Ma, P. Å. Malmqvist, T. Müller, A. Nenov, M. Olivucci, T. B. Pedersen, D. Peng, F. Plasser, B. Pritchard, M. Reiher, I. Rivalta, I. Schapiro, J. Segarra-Martí, M. Stenrup, D. G. Truhlar, L. Ungur, A. Valentini, S. Vancoillie, V. Veryazov, V. P. Vysotskiy, O. Weingart, F. Zapata and R. Lindh, *J. Comp. Chem.*, 2016, **37**, 506.

14 L. Ungur and L. F. Chibotaru, *Chem. Eur. J.*, 2017, **23**, 3708.

15 L. Ungur, M. Thewissen, J.-P. Costes, W. Wernsdorfer and L. F. Chibotaru, *Inorg. Chem.*, 2013, **52**, 6328.